



Royal Netherlands
Meteorological Institute
*Ministry of Infrastructure and the
Environment*

Delta-change approach for CMIP5 GCMs

Astrid Ruiter

De Bilt, 2012 | Trainee report

Delta-change approach for CMIP5 GCMs

Version 3

Date September 2012
Status Final



Universiteit Utrecht



Koninklijk Nederlands
Meteorologisch Instituut
Ministerie van Infrastructuur en Milieu

Delta-change approach for CMIP5 GCMs

Internship report
September, 2012
KNMI – Royal Netherlands Meteorological Institute

Astrid Ruiter
3232158
Master student Quaternary Geology and Climate Change
Department of Physical Geography
UU – Utrecht University

Under supervision of:
Jules Beersma (KNMI)
Adri Buishand (KNMI)
Raymond Sluiter (KNMI)
Maarten Zeylmans van Emmickhoven (UU)

Version 3

Koninklijk Nederlands Meteorologisch Instituut
PO Box 201, 3730 AE De Bilt, The Netherlands
Visiting address: Wilhelminalaan 10



Telephone +31 30 22 06 911
www.knmi.nl

Universiteit Utrecht
P.O. Box 80020, 3508 TA Utrecht, The Netherlands
Visiting address: Budapestlaan 4



Telephone + 31 30 253 3550
www.uu.nl

Table of Contents

Preface.....	3
1. Introduction	4
1.1 Study area.....	5
1.2 Observation data.....	6
1.3 Global climate model data.....	6
2. Delta change method	9
2.1 Advanced delta change method	9
2.2 Interpolation to a common grid.....	11
3. Results	15
3.1 Delta change method for 5-day precipitation sums.....	16
3.2 Return periods for maximum 10-day precipitation sums.....	19
4. Discussion.....	21
5. Conclusions & Future work.....	22
References.....	23
Appendix A: 90% quantiles of the CanESM2 and HadGEM2-ES models.....	26
Appendix B: Summary table for the summer period.....	29
Appendix C: Gumbel distribution for calculation of return periods.....	30

Preface

This report is written as a summary of the internship of Astrid Ruiten at the Royal Netherlands Meteorological Institute (KNMI) at the department of climate data and climate advice (KS-KA). This internship has been the final part of the master in Physical Geography at the University of Utrecht. The goal of this internship was to perform an individual research project, as a part of a larger project at a company or research institute to gain work experience.

This specific project is a continuation of a study of Saskia van Pelt, who is a PhD research student at Wageningen University and partly at KNMI. In the paper of Van Pelt et al., 2012, the method and her results are described. However, this is an internship report and it therefore only describes the method briefly, with some parts of the method which have been renewed or extended. Since more recent climate model data have been used for this study, the results will be different from the results described by Van Pelt et al., 2012, which will be described in the discussion. Also, the project is not finished yet. The project will be continued by Philip Kraaijenbrink who will start his internship in September 2012.

This internship has been performed under supervision of Maarten Zeilmans (UU) and Raymond Sluiter (KNMI). The project- and daily supervision has been carried out by Jules Beersma, in cooperation with Adri Buishand, Saskia van Pelt and Alexander Bakker. I would like to thank all of them for their help with the project and the interesting and pleasant time at the KNMI.

1. Introduction

The Netherlands has always been very vulnerable for high river discharges of the Rhine and Meuse rivers, which dominate the environment of the Netherlands as well as the upstream area. More than 50 million people live in the catchments of Rhine and Meuse and both are also very important for economic purposes as busy waterways (Disse and Engel, 2001). Therefore precipitation analysis are of major importance for economic and flood-risk assessment at present and for future protection. Most climate models show future changes in precipitation amount and distribution. Differences in temporal distribution could mean that the seasonal precipitation spread will change, which can result in dryer summers and wetter winter periods for the Rhine-Meuse area, or in an increase in extreme precipitation events (Frei et al., 2006; Fowler and Ekström, 2009). Most of the climate models show similar changes in temperature for northwestern Europe but changes in (extreme) precipitation are somewhat more uncertain (Frei et al., 2006; Reichler and Kim, 2008; Kysely and Beranova, 2009; Kysely et al., 2011).

This study describes an extended application of the advanced delta change method introduced by Van Pelt et al. (2012). The method is different from earlier delta change methods because it allows changes in extremes to be different from changes in the mean. Van Pelt et al. (2012) describe this method in detail and show the results of the future changes in extreme precipitation from RCM (Regional Climate Models) and GCM (Global Climate Models) ensembles of the CMIP3 (Coupled Model Intercomparison Project) models. The study of Van Pelt et al. (2012) shows the results of the method and a comparison between individual RCM outputs and the signal of the driving GCMs. In this study, a new generation of GCMs (for the CMIP5) has been used for the application of the advanced delta change method. In addition to the application to a newer generation of GCMs, the Meuse catchment area has been added to the study area. The method itself has not been changed but new research questions were formulated which this study tries to answer:

- Will the new generation of GCMs give significantly different results in future precipitation changes compared to the previous used models?
- Which GCMs show the largest and which the smallest changes in (extreme) precipitation?
- What is the effect of interpolation to a common grid on the extreme precipitation values?
- What is a suitable common grid for the Rhine-Meuse basin, given the spatial resolution of the CMIP5 GCMs and the study area?

The delta-change approach is a method to “downscale” global climate model data in order to use it as a future input for hydrological models and flood risk assessment. Different methods have been developed for downscaling climate models to use for precipitation and discharge calculations (Prudhomme et al., 2002; Te Linde, 2010). The advanced delta change method is a relatively simple and cheap method to use global or regional climate models for extreme precipitation changes in a smaller scale area (catchment scale) and use this information for changes in discharges and flood risk assessment for a catchment scale area.

In the remaining part of this chapter, the study area and data are described. The input data, the precipitation observations are described in section 1.2 and the global climate models (GCM) outputs are described in section 1.3. Chapter 2 gives a brief description of methods; first the delta-change approach in section 2.1, then the reason and testing method for assigning a common grid to the GCM data in section 2.2. In chapter 3 the results are described and chapter 4 discusses these results. This report ends with a conclusion about the method and the results and recommendations for future work.

1.1 Study area

The river Rhine, with a total length of 1230 km, is the longest river of western Europe. The Rhine originates in the Swiss Alps, and has a total basin area of 185 000 km². It is fed by glacier melt, snow melt and rainfall. The annual mean discharge (calculated over 1901-2000) at Lobith is 2 200 m³ s⁻¹ and the discharge corresponding the Dutch design discharge, an estimated 1250-year return level, is 16 000 m³ s⁻¹. This level (originally established by the Becht Committee in 1977) is evaluated every 5-years as a part of the flood protection management of the Delta Committee (Leander, 2009). In addition to the Rhine, the Meuse area is included in this study. The river Meuse originates on the plateau of Langres in northeastern France and is mainly fed by rainfall. The total basin area upstream of Borgharen is 21 000 km².

Although in this study the advanced delta change method is applied to the Rhine and Meuse basins, it can be applied elsewhere as long as daily precipitation and temperature observation data, with sufficient spatial density, are available. At the time of writing, there are plans to collaborate with German and Czech partners. Some preparations have already been taken to apply the same method and the same GCMs, to other large river basins relevant for Germany and the Czech Republic.

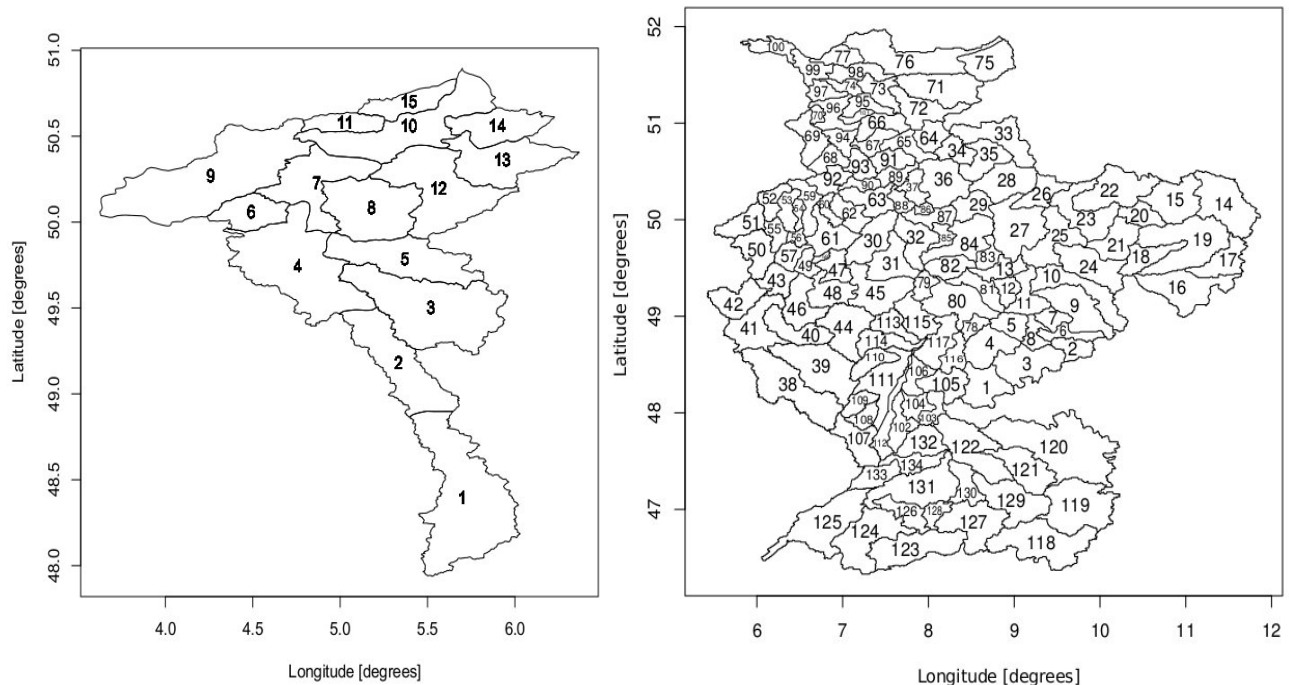


Figure 1: (A) The Meuse catchment with 15 individual subcatchments (after; Leander, 2009) and (B) the Rhine area with a total of 134 subcatchments (after; De Wit and Buishand, 2007). Note that in some older literature a different numbering is used for the Meuse basin.

1.2 Observation data

The delta-change approach requires observation data for the entire study area that serves as the basis for the method. The CHR-OBS dataset (International Commission for Hydrology of the Rhine basin; Eberle et al., 2005; De Wit and Buishand, 2007) have been used for the Rhine area. This dataset consists of area-average daily mean precipitation observations aggregated to 134 sub-catchments that can be used for hydrological modeling (by HBV; Hydrologiska Bryans Vattenblansavdelning) (Figure 1B). The CHR-OBS dataset is available for the period 1961 - 1995.

The Meuse area is subdivided into 15 HBV sub-basins (Figure 1A). Daily area-average mean precipitation observations for these sub-basins are available for the period 1961 - 2008. The data of French and Belgium meteorological surveys have been collected and interpolated to the HBV sub-basins by Buishand and Leander (2011).

Both Rhine en Meuse sub-catchments are combined into a single observation data-set. The period of the total 149 sub-basins is from 1961 - 1995. This is a 35-year period, which includes two extreme precipitation events in 1993 (December) and 1995 (January) (Ulbrich and Fink, 1995; Leander, 2009).

Observed and gridded precipitation and temperature data for the Czech Republic (CHMI-OBS) are available via Martin Hanel (from Czech University of Life Sciences Prague) and can be used for the planned future extension of this method to the Czech Republic.

1.3 Global climate model data

This study makes use of the GCM simulations from the CMIP5 archive. These are the latest GCM simulations available and they are analyzed for the upcoming IPCC assessment report (due 2013). Van Pelt et al. (2012) used GCM simulations from the previous CMIP version (i.e. CMIP3). To explore different possible futures the GCMs are 'forced' with different emission scenarios (which in turn depend on on different scenarios for socio-economic development and mitigation policies). Both in this study and Van Pelt et al. (2012), a single forcing was used. In this study the so called RCP4.5¹ (Representative Concentration Pathways; Meinshausen et al., 2010) and in Van Pelt et al. (2012) the SRES (Special Report on Emission Scenarios, IPCC) A1B emission scenario. Figure 2 compares for the different SRES and RCP forcings the corresponding CO₂ concentration as a function of time. Note that SRES A1B and RCP4.5 differ significantly in CO₂ concentration at the year 2100 (590 CO₂ eq. ppm for RCP4.5 vs. 780 CO₂ eq. ppm for the SRES A1B scenario). It is expected that these differences will also lead to differences in the results in this study and those in Van Pelt et al. (2012).

1 The 4.5 in RCP4.5 refers to a radiative forcing of 4.5 W/m² (based on a medium mitigation scenario, Taylor et al., 2009).

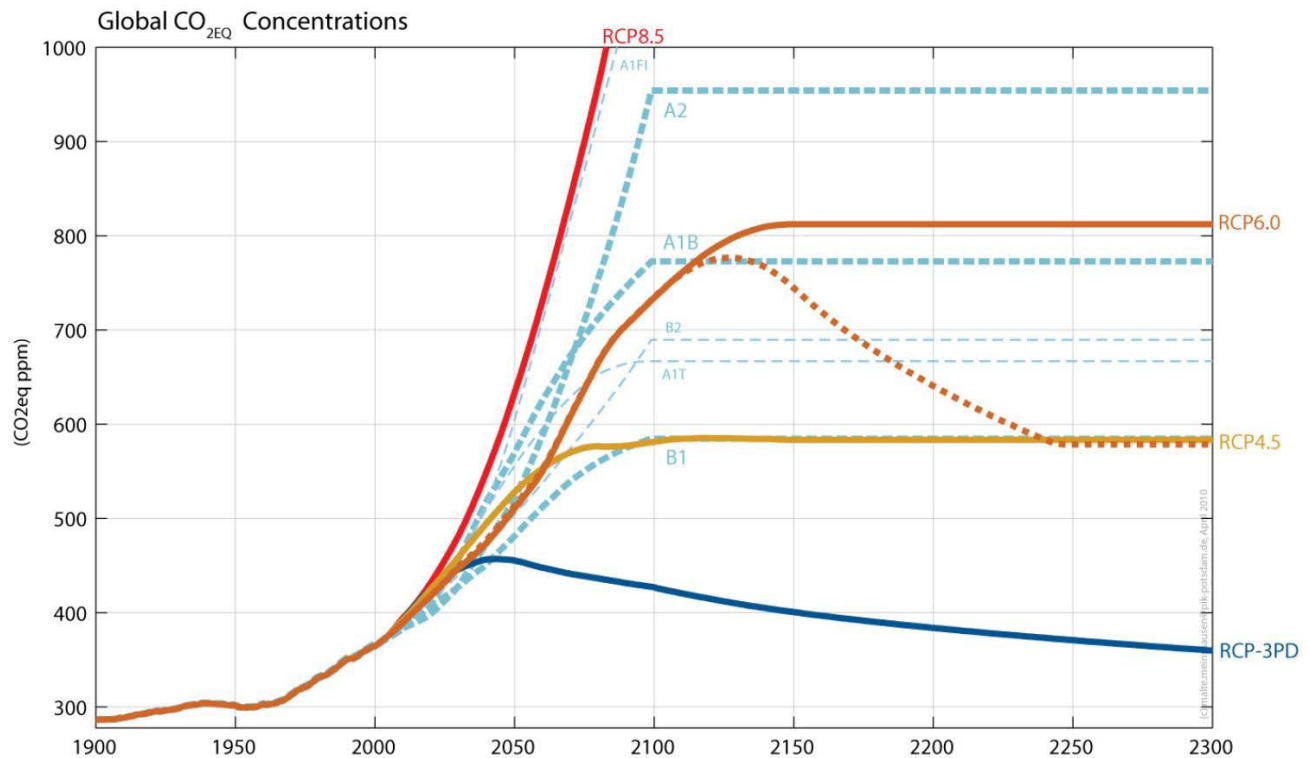


Figure 2: Comparison in terms of equivalent global CO₂ concentrations of SRES emission scenarios (B1, B2, A1T, A1B, A1F1, A2) used in CMIP3 simulations and RCPs (RCP-3PD, RCP4.5, RCP6.0 and RCP8.5) used as forcings for CMIP5 simulations (Lee, 2011).

A total of 38 out of 109 available RCP4.5 GCM model runs has been used in this study. The total of 38 model runs consists of 15 different GCM simulations with each between 1 and 9 model runs (Table 1). Daily precipitation data of the 38 model runs were all available for the three periods, commonly used in hydrological modeling; 1961-1995 (in a historical run), 2021-2050 and 2071-2100. In the remaining part of this report the period 1961-1995 is referred to as the “control period” and the period 2071-2100 as the “future period”. Note that the model data for the 2021-2050 period, was also made available and prepared but not further used in this study.

The GCMs are all available in Cartesian latitude-longitude grid, but the grid size and grid cell reference are different for each model. The majority of the models has a 365-day calendar, which is also known as 'no leap' because leap days are not included and each year has 365 days. Some of the models have a standard (gregorian) calendar, which includes the leap days. The HadGEM2-ES GCM is the only model which has a calendar of 360 days.

The GCM model outputs are available via the CMIP5 website (CMIP5, by Taylor, 2012) in NetCDF-files (Network Common Data Frame), which is a format that is easily usable for climate data, especially for large datasets (Unidata; Unidata Program Center, 2012).

	Model	Runs	Calendar	Institution	References
1	bcc-csm1-1	1	365-day	Beijing Climate Center, China Meteorological Administration	Wu et al., 2010
2	CanESM2	5	365-day	Canadian Centre for Climate Modelling and Analysis	Chylek et al., 2011
3	CCSM4	2	365-day	National Center for Atmospheric Research	Gent et al., 2011
4	CNRM-CM5	1	Standard	Centre National de Recherches Meteorologiques	Volodre et al., 2012
5	CSIRO-Mk3-6-0	9	365-day	Commonwealth Scientific and Industrial Research Organisation in collaboration with the Queensland Climate Change Centre of Excellence	Rotstayn et al., 2010
6	FGOALS-s2	3	365-day	LASG, Institute of Atmospheric Physics, Chinese Academy of Sciences	Juan et al., 2008
7	HadGEM2-ES	4	360-day	Met Office Hadley Centre	Collins et al., 2011
8	inmcm4	1	365-day	Institute for Numerical Mathematics	Volodin et al., 2010
9	IPSL-CM5A-LR	4	365-day	Institut Pierre-Simon Laplace	Dufresne et al., 2012
10	IPSL-CM5A-MR	1	365-day	Institut Pierre-Simon Laplace	Dufresne et al., 2012
11	MIROC-ESM	1	Standard	Japan Agency for Marine-Earth Science and Technology, Atmosphere and Ocean Research Institute	Watanabe et al., 2011
12	MIROC-ESM-CHEM	1	Standard	Japan Agency for Marine-Earth Science and Technology, Atmosphere and Ocean Research Institute	Watanabe et al., 2011
13	MPI-ESM-LR	3	Standard	Max Planck Institute for Meteorology	Raddatz et al., 2007; Jungclaus et al., 2010
14	MRI-CGCM3	1	Standard	Meteorological Research Institute	Yukimoto et al., 2011
15	NorESM1-M	1	365-day	Norwegian Climate Centre	Kirkevåg et al., 2008; Seland et al., 2008

Table 1: Different GCM simulations used in this study.

2. Delta change method

The delta change approach is a method that makes the output of GCMs useful for catchment scale analysis and hydrological modeling (which means that the GCM outputs are used indirectly). The method is based on the use of a change factor, the ratio between a mean value in the future and historical run. This factor is then applied to the observed time series to transform this series set into time series that is representative of the future climate.

2.1 Advanced delta change method

In the classical delta change method the transformation of the historical data makes only use of to changes in mean values. However, for flood risk assessments, for which extreme precipitation events are very important, the changes in the extremes, which may be different from those in the mean, should be taken into account as good as possible.

The advanced delta change method consists of a non-linear transformation of historical precipitation data. The advanced delta method takes into account the changes in mean and in extremes, to extract the climate signal from climate model outputs. This climate signal is applied on observation data to create a (transformed) future dataset. In the advanced delta change method 5-day precipitation sums are the starting point for the transformation. The 5-day sum is used to make the flood risk assessment possible, as extreme discharges occur as a result of extreme multiple-day precipitation amounts. Extreme multi-day sums between 4 to 20 days are considered to be relevant for the generation of extreme discharge for the Rhine area. Another reason for using a 5-day sum has to do with the practical issue that one year of 365 days can be subdivided into 73 non-overlapping 5-day periods.

The observed 5-day precipitation amounts P are transformed using:

$$\text{for } P < P_{90}^O : \quad P^* = a P^b \quad (1a)$$

$$\text{for } P > P_{90}^O : \quad P^* = \frac{\bar{E}^F}{\bar{E}^C} (P - P_{90}^O) + a (P_{90}^O)^b \quad (1b)$$

In which P is an historical 5-day sum, P^* the transformed (future) 5-day sum and a and b the transformation coefficients (parameters). In all equations and figures P^O and P^* represent the observed and transformed future precipitation data. Similar as the superscripts O and * represent the observed and transformed data, the superscripts C and F are representative for the control and future climates. The P_{90} is the 90% quantile, which is the threshold for which 90% of the probability distribution is below this value. E^C and E^F represent the excess variable of the control and future period of the GCMs. The amount E above the 90% quantile is called the excess (Equation 2).

$$E = P - P_{90} \quad (2)$$

Figure 3 is a schematic representation of the probability distribution of 5-day precipitation amounts for the observations and for the control and future GCM simulations together with their 60% and 90% quantiles and Excess.

The theoretical background for Equation (1b) in which the transformed precipitation linearly scales with the ratio of the future and control excess is given in Appendix A of Van Pelt et al. (2012). This linear scaling also avoids that unrealistically large precipitation amounts are generated, especially when b is larger than 1.

Similarly as for the 30% and 90% quantiles, 60% of the values are smaller than the 60% quantile. Note, that because of the skewness of the precipitation probability distribution (Figure 3) the 60% quantile is more representative for the mean than the median (which is the 50% quantile).

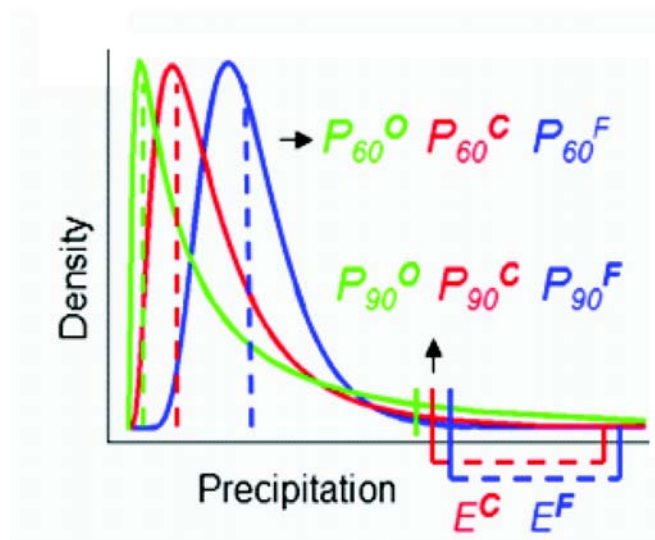


Figure 3: Schematic probability distribution of precipitation for observations and control and future data of the GCM simulations (Van Pelt et al., 2012).

The parameters a and b , which are used in Equation (1a and 1b), are calculated by the formulas (3) and (4) by eliminating a and then substituting b in Equation (1a).

$$b = \frac{\log\{g_2 P_{90}^F / (g_1 P_{60}^F)\}}{\log\{g_2 P_{90}^C / (g_1 P_{60}^C)\}} \quad (3)$$

$$a = P_{60}^F / (P_{60}^C)^b g_1^{(1-b)} \quad (4)$$

Correction factors (g_1 and g_2) are needed in Equation (3) and (4) and are calculated as:

$$g_1 = P_{60}^O / P_{60}^C \quad (5a)$$

$$g_2 = P_{90}^O / P_{90}^C \quad (5b)$$

These correction factors are needed to account for systematic differences in the 60% and 90% quantiles between the observations and the GCM control run and to ensure that in the transformation of the observations the relative changes of P_{60} and P_{90} derived from the GCM are reproduced.

To make the transformation as flexible as possible, the transformation coefficients vary spatially and/or seasonally. Therefore these coefficients are determined separately for each grid cell and each calendar month. To avoid sampling noise in these coefficients the underlying quantiles are smoothed by taking the monthly mean data of one-fourth of the previous, one-fourth of the next and half of the concerning month. To reduce sampling variability the median of b over all grid cells is uniformly used for all grid cells.

The mean excess for control and future periods, which is needed for the upper 10% of the probability distribution (as used in Equation (1b)), is described by:

$$\bar{E}^C = \frac{\sum E^C}{n^C} = \frac{\sum (P^C - P_{90}^C)}{n^C} \quad (6a)$$

$$\bar{E}^F = \frac{\sum E^F}{n^F} = \frac{\sum (P^F - P_{90}^F)}{n^F} \quad (6b)$$

In these equations E^C and E^F are the excesses of individual 5-day mums. n^C and n^F are the total number of excesses for the current and future climate. The mean excesses \bar{E}^C and \bar{E}^F are smoothed over time in a similar way as the quantiles.

The final step in the method is to apply a change factor to the daily observation data. The change factor is represented by:

$$R = P^* / P \quad (7)$$

The change factor is calculated for each 5-day sum period and is applied for each day within the 5-day period and is calculated for each grid cell separately. This way, a new data set of precipitation data was generated for each GCM. The same change factor R is also applied to the individual sub-basins within a grid-cell.

The entire method has been programmed in R, which is an open source software environment, performed for statistical computing and graphics (R Development Core Team, 2005).

2.2 Interpolation to a common grid

It was already noted in the previous section that the different GCMs have varying resolutions. For ease of comparison and to be able to use a common set of programs/scripts for applying the advanced delta change method to each GCM it is desirable to make use of a common (interpolated) grid. This was also done by Van Pelt et al. (2012) but they paid little attention to the fact that any interpolation smooths extreme values and thus also has an effect on extreme quantiles that play an important role in the advanced delta change method. This section describes the effect of interpolation on the individual quantiles and more importantly, on the quantile factor. As a result of this analysis, a new interpolated common grid was chosen. Figure 6 shows the new common grid boxes and the underlying 149 catchments of the concerning parts of the Rhine and Meuse area, which has been used as an input for the advanced delta change method.

In general, interpolation to a common grid causes smoothing of data. In particular the extreme values are smoothed, which in this study are of major importance. The effect of interpolation on the quantiles and quantile factors (as used in the delta change method) was studied for three models with different grid sizes. The three models used are: CanESM2 (grid size of 2.81 x 2.79 degree, a total of 9 grid cells), CCSM4 (grid size of 1.25 x 0.94 degree, a total of 35 grid cells) and HadGEM2-ES (grid size of 1.875 x 1.25 degree, a total of 18 grid cells). The effect of interpolation was investigated using the common grid of Van Pelt et al. (2012). This common grid contains 8 grid boxes and covers the Rhine area only. Therefore, the regridded data consists of 8 spatially varying values.

In the analysis both regridded and non-regridded model outputs were used to calculate the 30%, 60% and 90% quantiles for the control (1971-1995) and future (2071-2100) precipitation data. From this, quantile factors (which is the ratio of a quantile between the future and control periods for each grid cell and calendar month) have been calculated and compared.

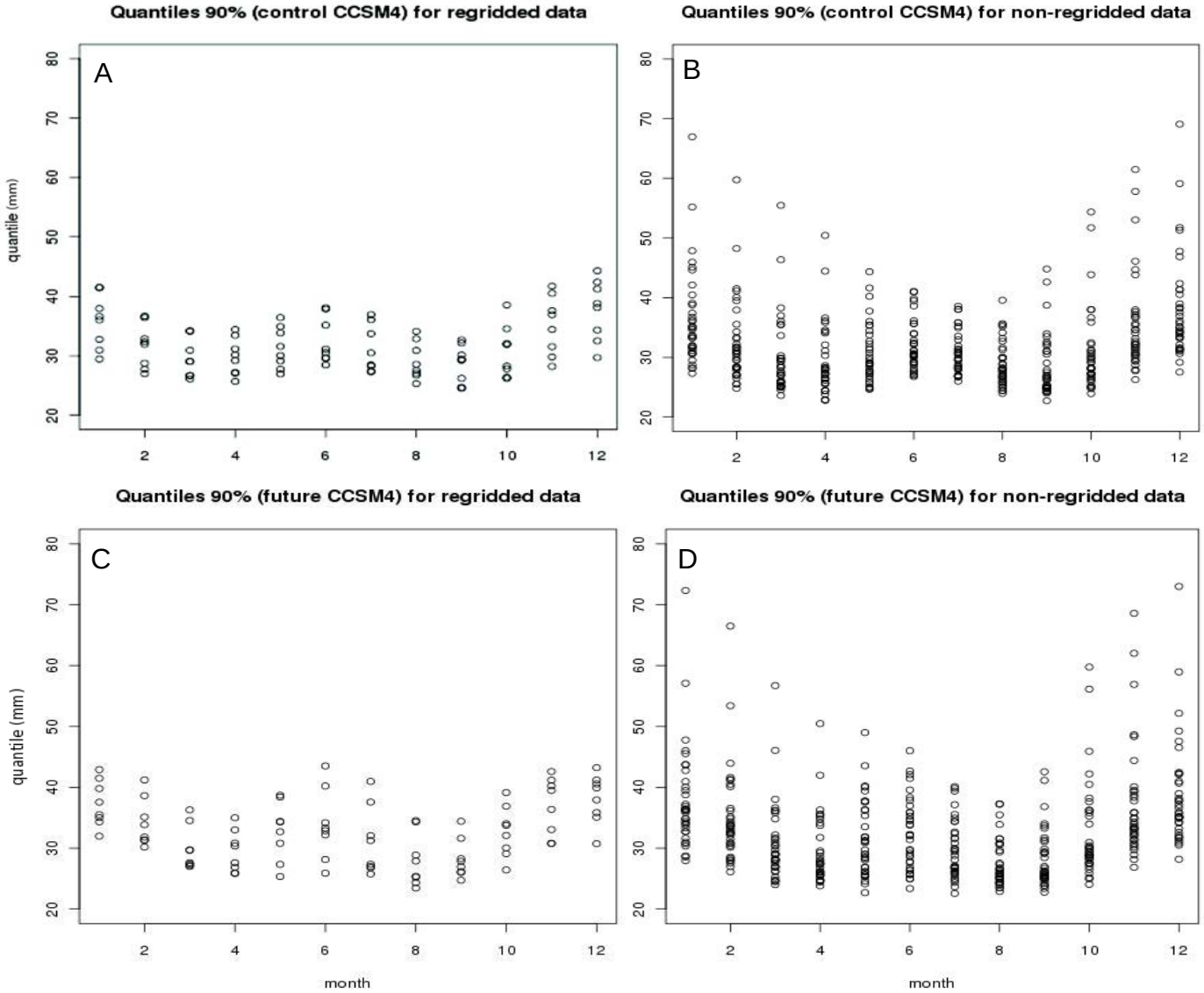


Figure 4: 90% quantile (in mm precipitation) of the CCSM4 model for the control (A and B) and future (C and D) period. The left panels (A and C) show the results of the regridded data (1 value per grid per month for 8 grid cells), the right panels (B and D) those for the results of the original 35 grid cells.

Figure 4 shows that for the CCSM4 model the individual 90% quantiles for the regridded data differ from those for the original grid cells. The figure shows the differences between the quantiles of the regridded and original data (A and C against B and D) but also the differences between control and future period (A and B against C and D). The largest differences are found for the winter period (months 10, 11, 12, 1, 2 and 3) in which the 90% quantiles of the original data show values up to 75 mm, while after interpolation these values are reduced to a maximum of only 45 mm. The difference between control and future periods is very small. Because of this small difference, the quantile factor (Figure 5) is generally around 1.0, both for the regridding and non-regridded data. The differences between the quantile factors of regridded and non-regridded values are relatively small, and especially the difference in the average for the summer (red line) and winter (blue line) periods is very small. Because the quantile factor is used in the transformation rather than the individual quantiles, the differences between the quantiles themselves are not of major influence on the method.

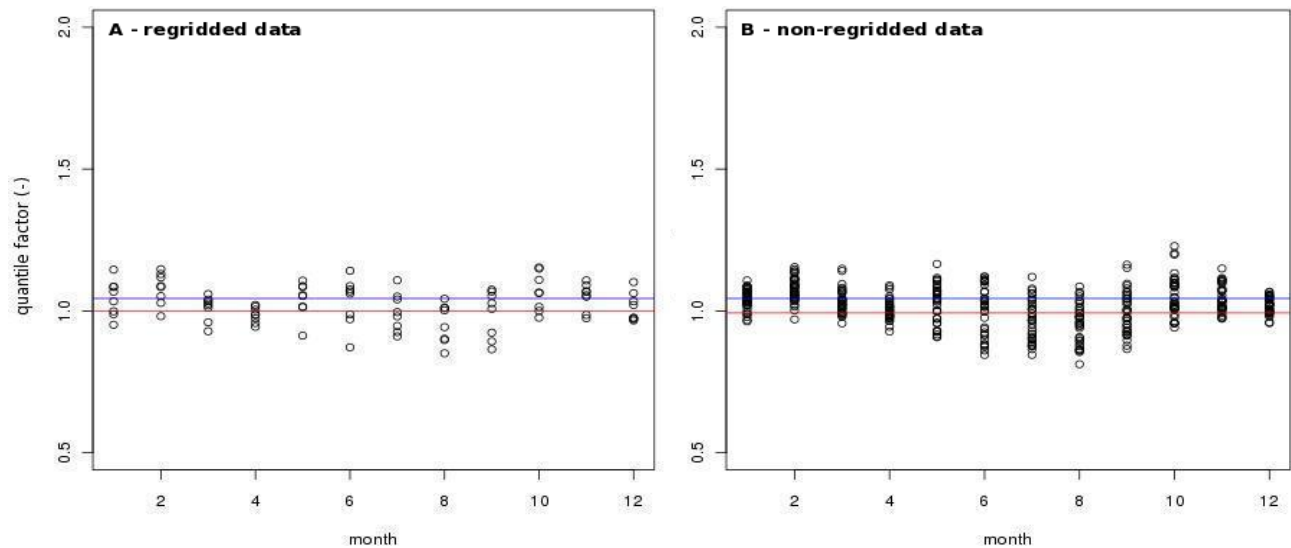


Figure 5: 90% quantile factor of the CCM4 model. At the left graph (A), the results of the regridded data have been shown. The right graph (B) shows the results of the original 35 grid cells. The blue line represents the winter mean (both 1.044) and the red line the summer mean (1.000 vs. 0.993).

The 90% quantiles for the CanESM2 and HadGEM2-ES regridded and original data show similar results and can be found in Appendix A.

These results, in combination with the desire to use a common grid for all GCMs, a new common grid of 1.2° latitude by 2° longitude was chosen. This grid is based on the mean size of all GCM grid resolutions in relation to the Rhine and Meuse basins (and Czech Republic). A grid with too large grid cells will have a too low spatial resolution which diminishes the ability to distinguish regional differences within the region of application. On the other hand, when the grid size becomes too small, an artificial accuracy will be introduced.

For the common 1.2° latitude by 2° longitude grid, currently 8 grid cells on the x axis, ranging from 4° to 20° E and 5 grid cells on the y axis, from 46° to 52° N (Figure 6) were interpolated, covering the Rhine and Meuse basins and the Czech Republic.

Only the westernmost 14 gridboxes, covering the Rhine and Meuse, were used in this study. The centroid of the individual catchments determines to which gridbox it is assigned. One exception is made for the most southern catchment of the Meuse (nr 1 in Figure 1A), which has been assigned to gridbox 7 as well, even though the centroid of this gridbox is located just south of the gridbox.

The interpolation to the common grid cells was performed using the program CDO (Climate Data Operators). This program has been developed by the Max-Planck-Institute for Meteorology of which version 1.0.6 (December 2006) was used in this study. Ferret is a similar program which can be used and has been used by Van Pelt (pers. comm.). This program uses the same interpolation technique (and gives the same results), has useful parts by easy commands to show the changes in grid, and it makes an automatic log-file. However, each model needs to be interpolated separately which increases the amount of work and the chance of (typographic) errors. With CDO, the NetCDF-files were interpolated using a standard bilinear interpolation technique (*cdo remapbil*) for the three selected time periods (1961-1995, 2021-2050 and 2071-2100).

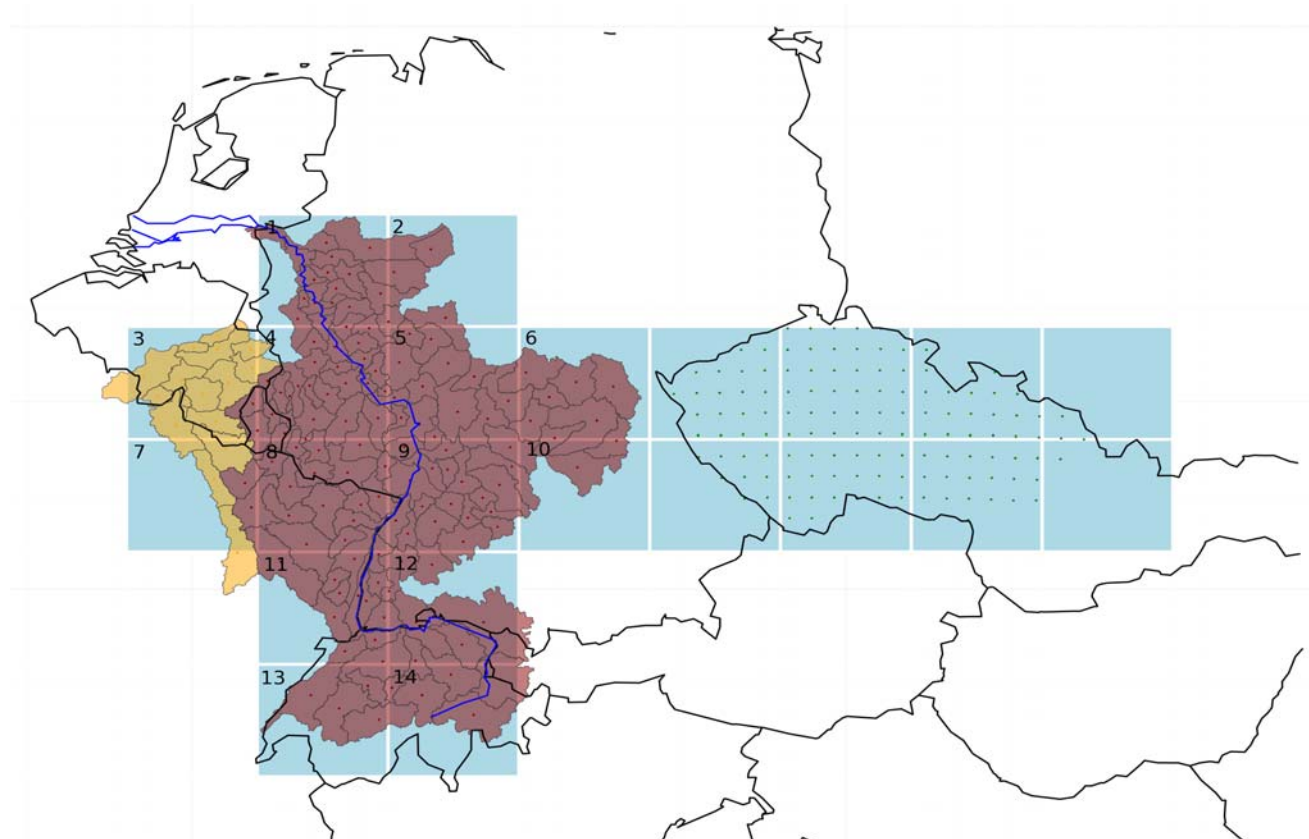


Figure 6: Study area with Rhine basin upstream from Lobith (red), Meuse basin upstream from Borgharen (yellow) and Czech Republic (green dots) with common grid (blue boxes).

3. Results

For the 38 RCP4.5 GCM simulations, the method was applied and a summary of the changes in the 30%, 60% and 90% quantiles and the excess is shown in Table 2. For completeness, the a and b transformation coefficients and a performance index (PI) are included in this table.

	WINTER	run	P30	P60	P90	\bar{E}	a	b	PI
1A	bcc-csm1-1	r1i1p1	0,928	0,998	1,061	1,140	0,814	1,096	41,19
2A	CanESM2	r1i1p1	0,795	0,892	1,014	1,117	0,652	1,162	3,44
2B	CanESM2	r2i1p1	0,917	0,987	1,083	1,175	0,803	1,120	3,44
2C	CanESM2	r3i1p1	0,897	0,972	1,026	1,191	0,843	1,100	3,44
2D	CanESM2	r4i1p1	0,826	0,881	0,987	1,161	0,632	1,181	3,44
2E	CanESM2	r5i1p1	0,876	0,939	1,023	1,167	0,742	1,122	3,44
3A	CCSM4	r1i1p1	0,884	0,934	0,976	1,077	0,827	1,092	9,03
3B	CCSM4	r2i1p1	0,687	0,816	0,931	1,077	0,622	1,149	9,03
4A	CNRM-CM5	r1i1p1	1,067	1,122	1,125	1,138	1,096	1,012	3,93
5A	CSIRO-Mk3-6-0	r10i1p1	0,841	0,933	1,040	1,169	0,740	1,107	5,75
5B	CSIRO-Mk3-6-0	r1i1p1	0,941	1,010	1,046	1,113	0,879	1,087	5,75
5C	CSIRO-Mk3-6-0	r3i1p1	0,757	0,865	0,969	1,080	0,650	1,162	5,75
5D	CSIRO-Mk3-6-0	r4i1p1	0,882	0,952	1,039	1,072	0,772	1,126	5,75
5E	CSIRO-Mk3-6-0	r5i1p1	1,019	1,049	1,079	1,070	0,973	1,069	5,75
5F	CSIRO-Mk3-6-0	r6i1p1	0,768	0,904	1,019	1,089	0,674	1,158	5,75
5G	CSIRO-Mk3-6-0	r7i1p1	0,922	0,981	1,061	1,104	0,861	1,088	5,75
5H	CSIRO-Mk3-6-0	r8i1p1	0,971	1,024	1,080	1,097	0,908	1,075	5,75
5I	CSIRO-Mk3-6-0	r9i1p1	0,830	0,939	1,032	1,133	0,747	1,117	5,75
6A	FGOALS-s2	r1i1p1	0,928	0,996	1,055	1,154	0,892	1,087	-
6B	FGOALS-s2	r2i1p1	0,889	0,970	1,024	1,037	0,806	1,092	-
6C	FGOALS-s2	r3i1p1	0,797	0,898	1,016	1,141	0,671	1,149	-
7A	HadGEM2-ES	r1i1p1	1,236	1,197	1,133	1,020	1,388	0,943	-
7B	HadGEM2-ES	r2i1p1	0,644	0,816	0,970	1,135	0,488	1,251	-
7C	HadGEM2-ES	r3i1p1	0,676	0,816	0,959	1,110	0,541	1,299	-
7D	HadGEM2-ES	r4i1p1	0,459	0,714	0,925	1,111	0,323	1,313	-
8A	inmcm4	r1i1p1	0,880	0,936	1,020	1,145	0,775	1,098	19,72
9A	IPSL-CM5A-LR	r1i1p1	1,032	1,052	1,086	1,131	1,001	1,056	17,92
9B	IPSL-CM5A-LR	r2i1p1	0,694	0,824	0,970	1,161	0,558	1,182	17,92
9C	IPSL-CM5A-LR	r3i1p1	0,820	0,934	1,034	1,152	0,695	1,138	17,92
9D	IPSL-CM5A-LR	r4i1p1	0,962	0,970	1,028	1,161	0,812	1,129	17,92
10A	IPSL-CM5A-MR	r1i1p1	0,748	0,866	1,004	1,199	0,607	1,174	-
11A	MIROC-ESM	r1i1p1	1,025	1,098	1,077	1,105	1,107	1,005	29,37
12A	MIROC-ESM-CHEM	r1i1p1	0,977	1,038	1,057	1,103	0,999	1,033	30,39
13A	MPI-ESM-LR	r1i1p1	0,936	0,979	1,026	1,070	0,889	1,059	8,19
13B	MPI-ESM-LR	r2i1p1	0,983	1,035	1,047	1,134	0,968	1,042	8,19
13C	MPI-ESM-LR	r3i1p1	0,930	1,043	1,073	1,118	0,918	1,056	8,19
14A	MRI-CGCM3	r1i1p1	1,031	1,073	1,084	1,110	1,020	1,027	3,14
15A	NorESM1-M	r1i1p1	0,880	0,969	1,058	1,162	0,798	1,094	-
	MEAN GCM's		0,877	0,959	1,033	1,122	0,802	1,112	10,724
	Min GCMs		0,459	0,714	0,925	1,020	0,323	0,943	3,140
	Max GCMs		1,236	1,197	1,133	1,199	1,388	1,313	41,190

Table 2: Relative changes in 30%, 60% and 90% quantiles and mean excess (resp. P30, P60, P90 and \bar{E}) for the 5-day precipitation sum in winter, after transformation by delta change approach. Also the change factors a and b are included in this table and a Performance Index (Wang, 2012) is shown in the last column. The colours indicate the highest (red) and lowest (blue) 5 values of the variables.

3.1 Delta change method for 5-day precipitation sums

Some of the results which are shown in Table 2 are plotted in Figure 7. In this figure, the 30%, 60% and 90% quantile factors (ratio between future and control period, respectively P^F_{30}/P^C_{30} , P^F_{60}/P^C_{60} and P^F_{90}/P^C_{90}) calculated directly from the GCMs are plotted against those calculated from the transformed observations. The different numbers represent the different GCMs and their model runs, the labels are shown in the first column of Table 2. The graph shows an almost perfect correspondence in all three quantile factors. This means that the applied transformation reproduces the future changes in these quantiles very well. Particularly in summer, the relation is stronger for the 60% and 90% quantile than for the 30% quantile (see Figure 7 and 8). This is likely a result of the delta change transformation, in which the 30% quantile is not explicitly used.

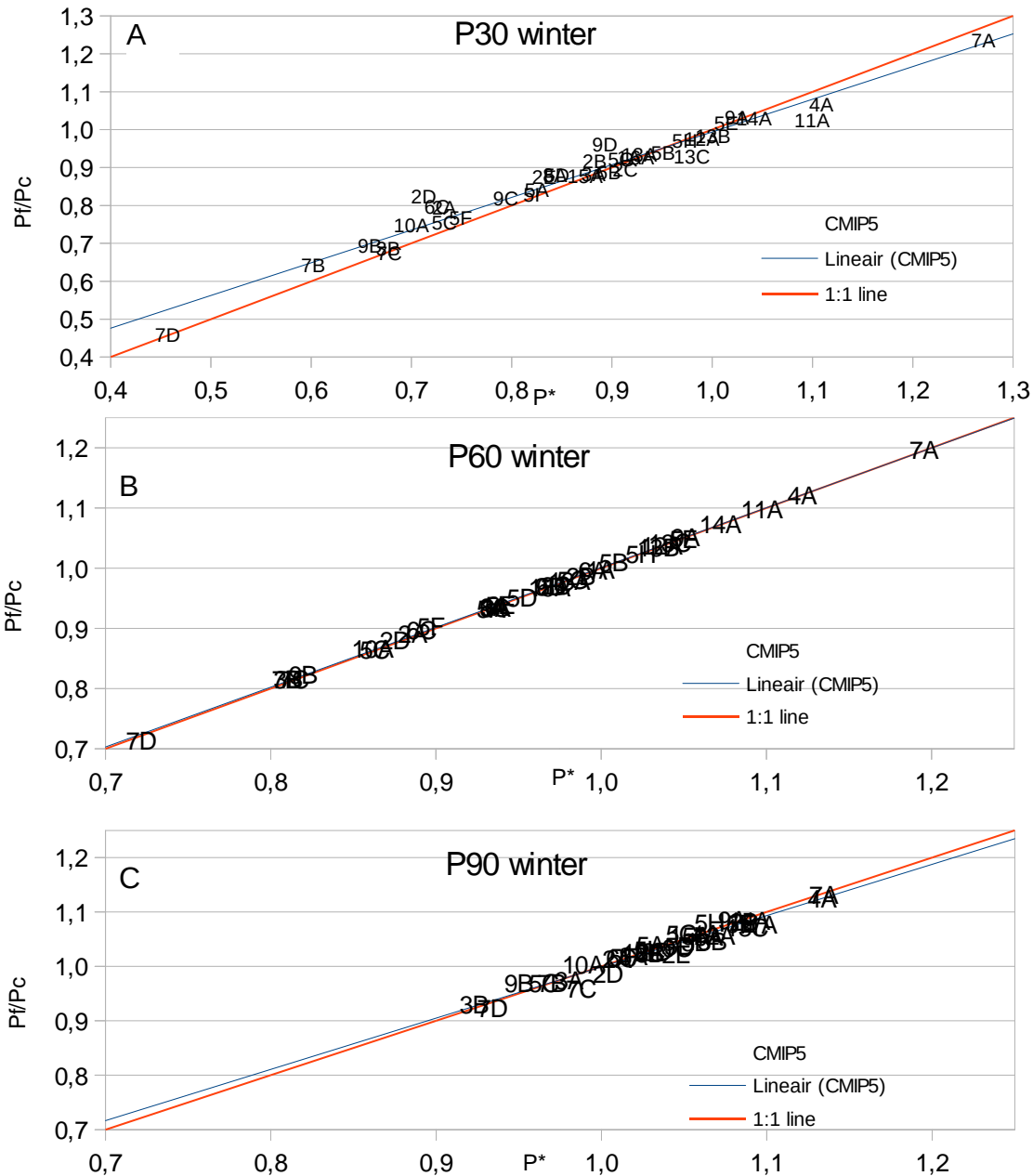


Figure 7: The 30%, 60% and 90% quantile factor (the ratio between P^F and P^C) vs the transformed observation data for the winter period. Note the differences in scale.

Winter

The mean of P_{90}^F / P_{90}^C for all GCM's (see Table 2) for the winter period is 1.03, which means an increase in the precipitation 90% quantile of 3%. The five lowermost model results are highlighted in blue, and the five highest values in red. An interesting result is that the HadGEM2-ES model shows the most variety and gives the minimal as well as maximal values for P_{90}^F / P_{90}^C , run 4 (7D in Figure 7) has the lowest value of 0.925 while run 1 (7A in Figure 7) results in the highest value of 1.13.

The 60% quantile is a representative value of the mean of the precipitation distribution. A value below 1 means that the total mean in precipitation will decrease in the future. Table 2 shows a value of 0.959, i.e. a decrease of 4,1%, for the 60% quantile in winter. Both 30% and 60% quantiles show a decrease in quantile factor (Figure 7A and 7B). The decrease in 30% quantile factor means that the driest parts of the precipitation distribution will become dryer. This 30% quantile has been included in the analysis to get a better insight in the dry part of the probability distribution of the precipitation. Since the results in Table 2 show a non-linear change in quantiles, the non-linear transformation is justified.

Summer

The P_{90}^F / P_{90}^C for the summer period (Figure 8, and the Table in Appendix B) shows a larger increase than for the same quantile averaged over all GCMs for the winter period; 1.09, an increase of 9% vs an increase of 3% for the winter period (Table 2). All models show an increase in the 90% quantile factor for the summer period, ranging from 1.03 for an IPSL-CM5A model to a maximum value of 1.13 for the HadGEM2-ES model, run 2 and 3 (7B and 7C). In comparison with the winter period, the inter model range between the different quantile factors is much smaller during the summer period (note the differences in scale of the x-axis between winter and summer (respectively Figures 7 and 8)). The change in quantile factors of P30 and P60 are similar to those for P90. The summer period shows higher values (i.e. larger increases) and a smaller range between the different models.

The changes in the mean excess (\bar{E}) are shown in Table 2. The mean increase in the excess in winter is 12.2%, with an overall range between + 2% and almost 20%. So in contrast to the changes in the quantiles (i.e. the quantile factors) no decreases are found for any of the models. The highest value for excess is by IPSL-CM5A-MR model, which is 1.199, while the lowest value for excess is 1.020 by the first run of the HadGEM2-ES model.

The range in the resulting values, for both summer and winter period (Table 2), increase from excess, towards the quantiles 90%, 60% and 30%. This means that the uncertainty increases towards the 30% quantile. The total range of the 30% quantile is 0.777, which results in quantiles vary from 0.459 for the HadGEM2-ES model (run 4) towards 1.236 for the HadGEM2-ES model (run 2). As well for the 90% and 60% quantiles, the HadGEM2-ES shows the largest variability. The excess shows a different pattern. With exception of HadGEM2-ES run 1, all HadGEM2-ES model runs show similar values.

As expected large increases (decreases) of P60 and P90 typically correspond to large (low) values of a. And, large (small) differences between the changes of P60 and P90 lead to values larger than (close to) 1. Quite often large values of a are accompanied by low values of b and vice versa. From this we may conclude that the largest increases of P60 and P90 are more linear in character than the largest decreases of P60 and P90. A similar result is also found for the summer period (see Appendix B). At this moment we don't have a logical explanation for this negative correlation between the parameters a and b. The Performance Index (*PI*) is a method of Wang, (2012), to order the different GCMs in their performance (the models that represent the current climate best have the lowest values). Wang (2012) shows how well the GCMs can reproduce the present climate to be able to order the results of the different GCMs for the KNMI next scenarios. Not all models used by Wang (2012) are included in this study and vice versa. The values in the last column of Table 2 represent PI values of Wang (2012), averaged over the winter period. Every model is represented by one single value and no difference in model runs have been made. Unfortunately, the HadGEM2-ES model is not included in the study of Wang (2012), which would have been very interesting because this model shows the largest variation

within the results. The table does not show a correlation between PI values and any of the other results in Table 2.

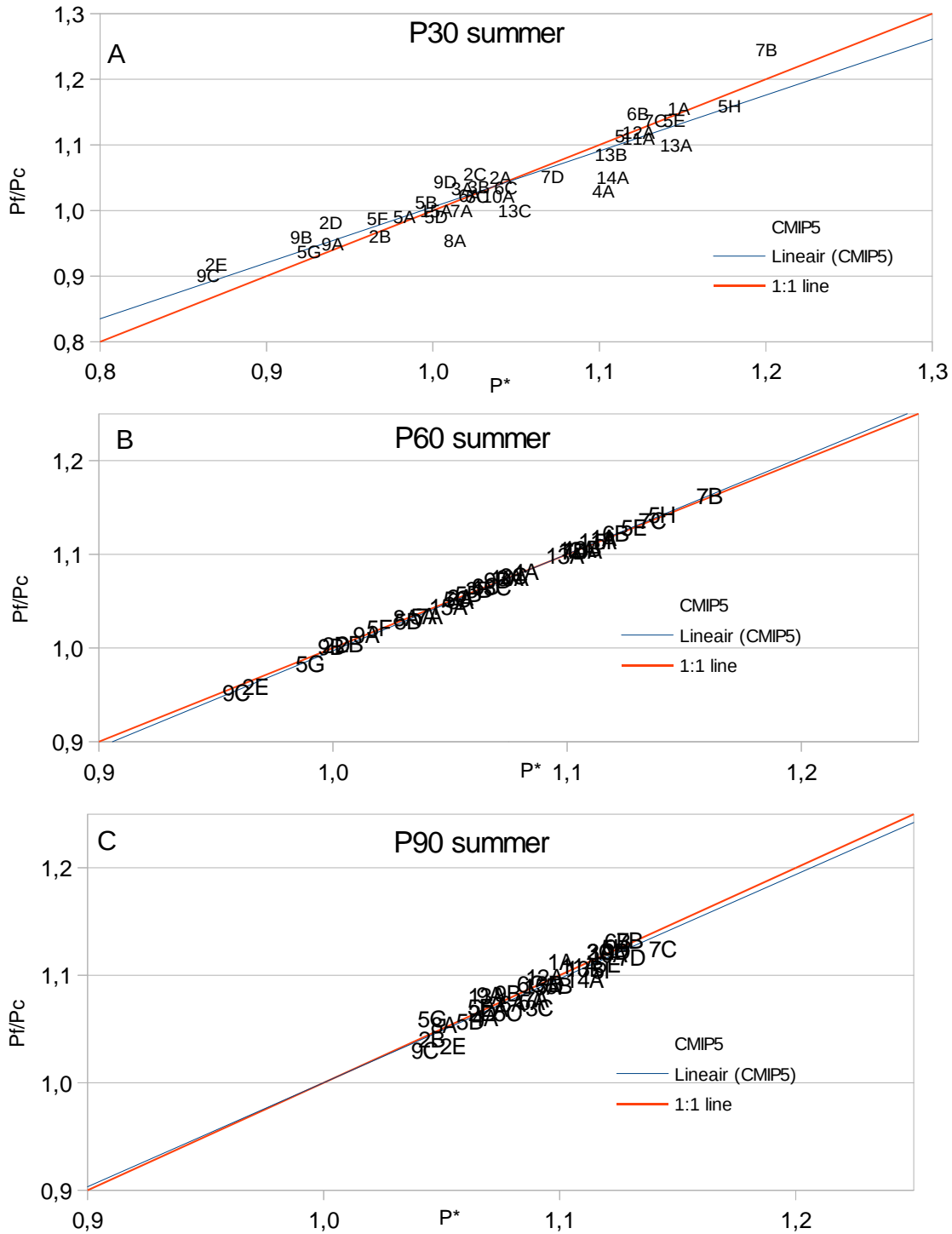


Figure 8: The 30%, 60% and 90% quantile factor (the ratio between Pf and Pc) vs the transformed observation data for the winter period. Note the differences in scale.

Table 3 shows the results of the analysis of the CMIP3 models by Van Pelt et al. (2012). This shows for the 90% quantile a mean change of 8.5%.

The CMIP3 data, which are forced by the A1B emission scenario, (Van Pelt et al., 2012) show an increase in P_{90} for all models. This is in contrast to the CMIP5 data, which are forced by a RCP4.5 forcing, in which 8 out of the 38 models show a decrease in 90% quantile of the precipitation. The mean change of the winter 90% quantiles of all GCMs for the CMIP3 is also higher than for the CMIP5 GCMs (8.5% vs. 3%). The range between the different model outputs is for all variables (P_{60}^F/P_{60}^C and P_{90}^F/P_{90}^C) smaller for the CMIP3 results compared to the CMIP5 results.

	WINTER	P60	P90	\bar{E}
	CGCM3.1T63	1,1	1,11	1,22
	CNRM-CM3	0,97	1,04	1,28
	CSIRO-Mk3.0	1,01	1,05	1,17
	ECHAM5r1	0,98	1,04	1,25
	ECHAM5r3	1,11	1,15	1,11
	GFDL-CM2.0	1,04	1,11	1,21
	GFDL-CM2.1	1,05	1,1	1,41
	HADCM3Q0	1,12	1,17	1,35
	HADCM3Q3	1,07	1,12	1,2
	IPSL-CM4	0,89	1,01	1,36
	MIROC3.2	0,94	1,03	1,19
	MIUB	0,95	1,09	1,24
	MRI-CGCM2.3.2	1,05	1,09	1,34

Table 3: Relative changes in 60% and 90% quantiles and mean excess (resp. P_{60} , P_{90} and \bar{E}) for the 5-day precipitation sum in winter, based in CMIP3 A1B simulations (after; Van Pelt et al., 2012).

3.2 Return periods for maximum 10-day precipitation sums

Return level plots of the maximum 10-day precipitation for the CMIP5 GCMs used in this study are shown in Figure 9A. A similar figure for the CMIP3 simulations used by Van Pelt et al. (2012), is given in Figure 9B. The 10-day annual maxima are in both figures derived from the transformed historical time series (using the advanced delta change method). Note that in these plots, the horizontal axis, i.e. the return period, corresponds to the scale of a Gumbel distribution (see Appendix C for details).

Both graphs show a very similar change in higher values and a larger range between the values for the longer return periods. For the CMIP3 GCMs, the 50 year return period is between 110 and 150 mm for the different model runs. For the CMIP5 GCMs this value ranges from 120 up to 170 mm. The largest 10-day precipitation amounts are generated by the HadQ0 model for CMIP3 and the CSIRO-Mk3-6-0 for the CMIP5 GCMs. Although both types of model simulations show similar changes in future return levels, a proper comparison between the future return levels of the 10-day precipitation maxima of the CMIP5 and CMIP3 simulations can not be made because: a) The CMIP3 A1B and CMIP5 RCP4.5 simulations differ in climate forcings (i.e. CO_2 concentration, see Figure 2) and b) the 10-day precipitation amounts in this

study involve both the Rhine and Meuse basins while the 10-day precipitation amounts in Van Pelt et al. (2012) refer to the Rhine basin only. The precipitation in the Meuse area is a little higher than in the Rhine basin which causes the 50-year return level of the observations (the black lines) to decrease from 119 mm in panel A to 113 mm in panel B.

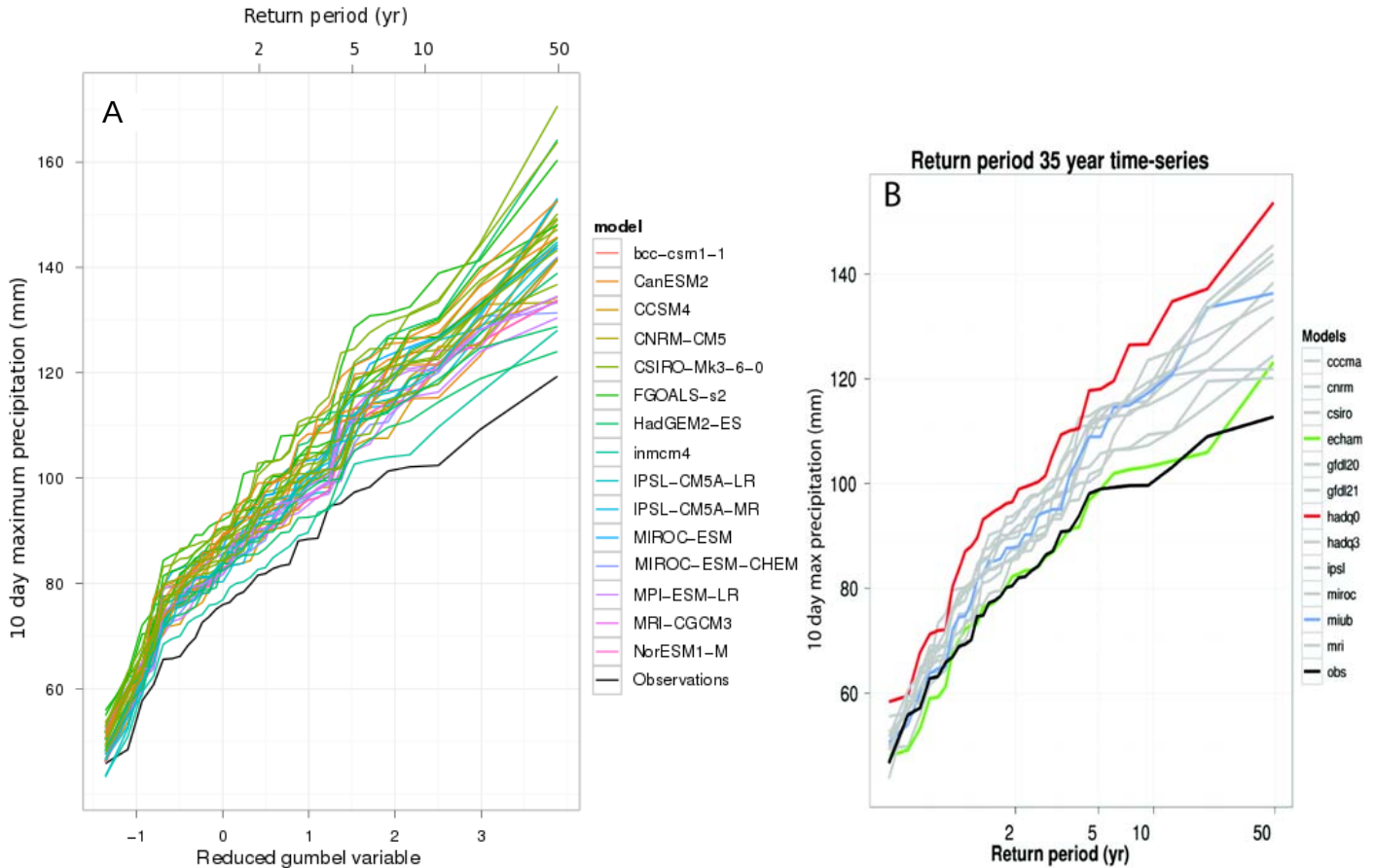


Figure 9: (A) Return levels of 10-day maximum precipitation amounts for CMIP5 RCP4.5 simulations and (B) CMIP3 A1B simulations (after Van Pelt et al., 2012) for the end of the 21st century compared with the return levels for the observations (the black line).

4. Discussion

The advanced delta change approach resulted in a reliable transformed observation dataset for the future period representative of 2071 and 2100. All 38 analyzed CMIP5 RCP4.5 GCM simulations show an increase in extreme precipitation around 2100. The 50-year return levels for 10-day precipitation sums are around 140 mm. For the CMIP3 A1B scenarios (Van Pelt et al., 2012) these 50-year return levels show a mean in max 10-day precipitation sum are around 10% lower. The individual quantile factors of the 60% and 90% and the excess values (Table 2) show a decrease in winter mean for CMIP5 in comparison with the CMIP3 results. Even though the mean winter precipitation in this study is lower, compared to the study of Van Pelt et al. (2012), it still shows a mean increase in extreme precipitation of 12%.

Except for the differences between the CMIP3 and CMIP5 model simulations (see legend of Figure 9), more differences are present between the results of this study and the study of Van Pelt et al. (2012). This study is based on a larger study area. Except from having another reference observation dataset, the model outputs are regridded with a larger area which extend more towards the west. This might change the total precipitation amounts and could include more oceanic influences. However, this effect is presumably neglectable since the study area is large enough to smooth these small changes. This difference in study area causes an extra variability between both studies. For correct comparison between CMIP3 and CMIP5 climate models, the results of this study should be split between the Rhine and the Meuse catchments.

During this study a start has been made for using the 30% quantile for the method. This may provide a better insight in the dry part of the precipitation probability distribution. Although the future change in the 30% quantile is not an explicit element in the non-linear transformation, it is still considered useful to analyze the reproduction of P30 in the transformed historical series since it gives an idea about how well the transformation works for the dryer (less wet) part of the precipitation probability distribution. Especially for GCM simulations in which there is a large reduction of precipitation (i.e. in summer drying).

The plume of the extreme 10-day precipitation amounts (Figure 9) is a useful way to show the variations between all different models (in this study for only one emission scenario). When all available models are included in this plume, the entire CMIP5 range of precipitation change will be covered. For hydrological modeling, using this extreme multi-day precipitation plume, only a small number of the CMIP5 model simulations can be selected to cover the entire range of climate models.

5. Conclusions & Future work

- The new generation of GCMs shows different results in future precipitation changes compared to the previous used models. The mean of the changes in excess, 90% and 60% quantiles are all lower for the CMIP5 climate model simulations (RCP4.5) than for the CMIP3 simulations (SRES A1B). This difference is at least partly caused by the difference in climate forcing. In contrast, the for the 10-day precipitation the largest return levels estimated are higher for the CMIP5 models than for CMIP3.
- The HadGEM2-ES model runs show the most extreme values for changes in 30%, 60% and 90% quantiles and excess, and therefore the largest changes in extreme precipitation.
- The effect of the interpolation to a common grid is significant for the individual quantiles, but for the quantile factors this effect is almost negligible. The advanced delta change method only uses the quantile factors and therefore the effect of interpolation to a common grid on the extreme precipitation values is not significant.
- A suitable common grid for the Rhine-Meuse basin and the Czech Republic, given the spatial resolution of the CMIP5 GCMs and the study area, has been chosen. This grid has a resolution of 1.2° longitude by 2° latitude (close to the average of all available GCMs) and is shown in Figure 5.

More research is needed to be able to use the 10% and 30% quantiles which might be relevant to adapt the advanced delta change method for drought studies.

The application of the advanced delta change method to other river basins including the use of CMIP5 GCM simulation forced by the other RCPs will be performed by the next intern. He will continue this study and generate time series to be used together with the next generation of KNMI climate scenarios (due autumn 2013) and especially for hydrological modeling purposes (in collaboration with RWS-Waterdienst and Deltares). To prepare the transformed (future) time series for hydrological modeling, the following subjects must be studied;

- The method must be extended with and applied to temperature data to be able to use the results for hydrological modeling.
- Include leap days in the transformed historical data-set to complete the time series (the scripts of Van Pelt (pers. comm.) already have this option).
- Apply the transformation on long term (3 000 to 20 000 year) precipitation data sets, which are generated by the KNMI-rainfall generator.
- Apply the method for the future period 2021-2050 and compare these results with the period 2071-2100. This might give more insight in the direct effect of different forcings.
- Distinguish between the results for the Rhine and Meuse catchments for better comparison between the changes for the delta change method based on CMIP3 (SRES A1B) and CMIP5 (RCP4.5) climate model simulations.
- Apply the advanced delta method on a other river basins and investigate the effect of using an average b parameter with an larger study area.
- Apply the advanced delta method on other GCM simulations (for example RCP6.0) for better comparison between CMIP3 and CMIP5 and the effect of different forcings and to cover the entire range of the climate signal.

References

- Aalders, P., Warmerdam, P.M.M. and Todfs, P.J.J.F., 2004. Rainfall generator for the Meuse Basin; 3,000 year discharge simulations in the Meuse basin. *Wageningen University, sub-department water resources; Report 124*.
- Bernstein, L., Bosch, P., Canziani, O., Chen, Z., Christ, R., Davidson, O., Hare, W., Huq, S., Karoly, D., Kattsov, V., Kundzewicz, Z., Liu, J., Lohman, U., Mannin, M., Matsuno, T., Mene, B., Metz, B., Mirza, M., Nicholls, N., Nurse, L., Pachauri, R., Palutikof, J., Parry, M., Qin, D., Ravindranath, N., Reisinger, A., Ren, J., Riahi, K., Rosenzweig, C., Rusticucci, M., Schneider, S., Sokona, Y., Solomon, S., Stott, P., Stouffer, R., Sugiyama, T., Swart, R., Tirpak, D., Vogel, C. and Yohe, G., 2007. Climate change 2007: Synthesis report, Intergovernmental Panel on Climate Change (IPCC), *Geneva, 1–52*.
- Buishand, T.A., and Leander, R., 2011. Rainfall generator for the Meuse; Extension of the base period with the years 1999-2008. *KNMI-publication; 196-V*.
- Chylek, P., Li, J., Dubey, M. and Lesins., G. 2011. Observed and model simulated 20th century arctic temperature variability: Canadian earth system model canasm. *Atmos Chem Phys Discuss 11: 22*.
- Collins, W.J., Bellouin, N., Doutriaux-Boucher, M., Gedney, N., Halloran, P., Hinton, T., Hughes, J., Jones, C.D., Joshi, M., Liddicoat, S., Martin, G., O'Connor, F., Rae, J., Senior, C., Sitch, S., Totterdell, I., Wiltshire, A. and Woodward, S., 2011. Development and evaluation of an Earth-System model-HadGEM2. *GMD 4(4):1051-1075*.
- De Wit, M.J.M. and Buishand, T.A., 2007. Generator of Rainfall And Discharge Extremes (GRADE) for the Rhine and Meuse basins. *Rijkswaterstaat RIZA report 2007.027/KNMI publication 218. Lelystad, The Netherlands*.
- Dissel, M., and Engel, H., 2001. Flood events in the Rhine basin: Genesis, influences and mitigation. *Natural Hazards, 23: 271-290*.
- Dufresne, J.L., Foujols, M.A., Denvil, S., Caubel, A. and Marti, O., 2012. Climate change projections using the IPSL-CM5 earth system model: from CMIP3 to CMIP5. *Clim Dyn*.
- Eberle, M., Buiteveld, H., Krahe, P. and Wilke, K., 2005. Hydrological Modelling in the River Rhine Basin, Part III: Daily HBV model for the Rhine basin. *Report 1451, Bundesanstalt für Gewässerkunde (BFG), Koblenz, Germany, 2005*.
- Frei, C., Schöll, R., Fukutome, S., Schmidli, J. and Vidale, P.L., 2006. Future change of precipitation extremes in Europe: Intercomparison of scenarios from regional climate models. *Journal of geophysical research, 111. 22 p*.
- Gent, P. R., Danabasoglu, G., Donner, L.J., Holland, M.M., Hunke, E.C., Jayne, S.R., Lawrence, D.M., Neale, R.B., Rasch, P.J., Vertenstein, M., Worley, P.H., Yand, Z.L. and Zhang, M., 2011. The Community Climate System Model version 4. *J. Climate*.
- Görge, K., Beersma, J., Brahmer, G., Buiteveld, H., Carambia, M., de Keizer, O., Krahe, P., Nilson, E., Lammersen, R., Perrin, C. and Volken, D., 2010. Assessment of climate change impacts on discharge in the Rhine river basin: Results of the RheinBlick2050 project, *International Commission for the Hydrology of the Rhine basin (CHR), Lelystad, Report no. I-23, 229 pp*.
- Juan, L., Bin, W., Hailong, L. and Yongqiang, Y., 2008. A New Global Four-Dimensional Variational Ocean Data Assimilation System and its Application. *Adv. Atmos. Sci., Vol. 25, NO. 4, 2008, 680-691*.

Jungclaus, J.H., Lorenz, S.J., Timmreck, C., Reick, C.H., Brovkin, V., Six, K., Segschneider, J., Giorgetta, M.A., Crowley, T.J., Pongratz, J., Krivova, N.A., Vieira, L.E., Solanki, S.K., Klocke, D., Botzet, M., Esch, M., Gayler, V., Haak, H., Raddatz, T.J., Roeckner, E., Schnur, R., Widmann, H., Claussen, M., Stevens, B. and Marotzke J., 2010. Climate and carbon-cycle variability over the last millennium. *Clim Past* 6(5):723-737.

Kirkevåg, A., Iversen, T., Seland, O., Debernard, J.B., Storelvmo, T. and Kristjansson, J.E., 2008. Aerosol-cloud-climate interactions in the climate model CAM-Oslo. *Tellus A* 60(3):492-512.

Kysely, J., and Beranova, L., 2009. Climate-change effects on extreme precipitation in central Europe: uncertainties of scenarios based on regional climate models. *Theor. Appl. Climatology* 95: 361-374.

Kysely, J., Gaal, L., Beranova, R., Plavcova, E., 2011. Climate change scenarios of precipitation extremes in Central Europe from ENSEMBLES regional climate models. *Theor Appl. Climatology* 104: 529-542.

Leander, R., and Buishand, T.A., 2007. Resampling of regional climate model output for the simulation of extreme river flows. *Journal of Hydrology*, 332: 487-496.

Leander, R., 2009. Simulation of precipitation and discharge extremes of the river Meuse in current and future climate. *Proefschrift aan Universiteit Utrecht*.

Lee, R., 2011. Extratropical storm tracks in some of the CMIP5 Models. *Presentation University of Reading*.

Lenderink, G., Buishand, A., and Deursen, W., 2007. Estimates of future discharges of the river Rhine using two scenario methodologies: direct versus delta approach. *Hydrology & Earth System Sciences*, 11(3): 1145-1159.

Meinshausen, M., Smith, S.J., Calvin, K., Daniel, J.S., Kainuma, M.L.T., Lamarqua, J-F., Matsumoto, K., Montzka, S.A., Raper, S.C.B., Riahi, K., Thomson, A., Velders, G.J.M. and van Vuuren, D.P.P., 2010. The RCP greenhouse gas concentrations and their extensions from 1765 to 2300. *Climate Change*, 109: 213-241.

R Development Core Team, 2005. A Language and Environment. *R Foundation for Statistical computing, Vienna, Austria*. <http://www.R-project.org>.

Raddatz, T.J., Reick, C.H., Knorr, W., Kattge, J., Roeckner, E., Schnur, R., Schnitzler, K.G., Wetzel, P. and Jungclaus, J., 2007. Will the tropical land biosphere dominate the climate-carbon cycle feedback during the twenty-first century? *Clim Dyn* 29(6):565-574.

Prudhomme, C., Reynard, N. and Crooks, S., 2002. Downscaling of global climate models for flood frequency analysis: where are we now? *Hydrological Processes*, 16: 1137-1150.

Reichler, T. and Kim, J., 2008. How Well Do Coupled Models Simulate Today's Climate? *Bull. Amer. Meteor. Soc.*, 89: 303-311.

Rotstayn, L., Collier, M., Dix, M., Feng, Y., Gordon, H., O'Farrell, S., Smith, I. and Syktus, J., 2010. Improved simulation of Australian climate and ENSO-related climate variability in a GCM with an interactive aerosol treatment. *Int. J. Climatology*, vol 30(7): 1067-1088.

Seland, O., Iversen, T., Kirkevåg, A. and Storelvmo, T., 2008. Aerosol-climate interactions in the CAM-Oslo atmospheric GCM and investigation of associated basic shortcomings. *Tellus A* 60(3): 459-491.

Taylor, K.E., 2012. Information about the CMIP5 experiments design and any CF and data output. *Program for Climate Model Diagnosis and Intercomparison, LLNL*. <http://cmip-pcmdi.llnl.gov/cmip5/>

Taylor, K.E., Stouffer, R.J. and Meehl, G.A., 2009. A Summary of the CMIP5 Experiment Design. *Program For Climate Model Diagnosis and Intercomparison*.

Taylor, K.E., Stouffer, R.J. and Boer, G., 2010. Addendum to the CMIP5 Experiment Design Document: A compendium of relevant emails sent to the modeling groups. *Program For Climate Model Diagnosis and Intercomparison*.

Te Linde, A.H., Aerts, J.C.J.H., Bakker, A.M.R. and Kwadijk, J.C.J., 2010. Simulating low-probability peak discharges for the Rhine basin using resampled climate modeling data. *Water Resources Research*, 46.

Ulbrich, U., and Fink, A., 1995. The January 1995 flood in Germany: Meteorological versus hydrological causes. *Phys. Chem. Earth* 20, nr 5-6: 439-444.

Unidata Program Center, 2012. Providing innovative data services and tools to transform the conduct of geoscience. *Unidata Program Center, Boulder, CO, United States*. <http://www.unidata.ucar.edu>.

Van Pelt, S.C., Beersma, J.J., Buishand, T.A., Van den Hurk, B.J.J.M. and Kabat, P., 2012. Future changes in extreme precipitation in the Rhine basin based on global and regional climate model simulations. *Hydrology and Earth System Science Discussions*, 9: 6533-6568.

Voldoire, A., Sanchez-Gomez, E., Salas y Melia, D., Decharme, B. and Cassou, C., 2011. The CNRM-CM5.1 global climate model: description and basic evaluation. *Clim Dyn*.

Volodin, E.M., Diansky, N.A. and Gusev, A.V., 2010. Simulating present-day climate with the INMCM4.0 coupled model of the atmospheric and oceanic general circulations. *Atmospheric and oceanic physics*, V.46, N4.

Wang, X., 2012. Performance Index (PI) analysis and bias of the CMIP5 models for the KNMI next scenarios. *KNMI-publications*.

Watanabe, S., Hajima, T., Sudo, K., Nagashima, T., Takemura, T., Okajima, H., Nozawa, T., Kawase, H., Abe, M., Yokohata, T., Ise, T., Sato, H., Kato, E., Takata, K., Emori, S. and Kawamiya, M., 2011. MIROC-ESM 2010: model description and basic results of CMIP5 20c3m experiments. *GMD* 4(4):845-872.

Wu, T.W., Yu, R.C., Zhang, F., Wang, Z., Dong, M., Wang, L., Jin, X., Chen, D. and Li, L., 2010. The Beijing Climate Center atmospheric general circulation model (BCC-AGCM2.0.1): description and its performance for the present-day climate. *Clim Dyn* 34: 123-147.

Yukimoto, S., Adachi, Y., Hosaka, M., Sakami, T., Yoshimura, H., Hirabara, M., Tanaka, T.Y., Shindo, E., Tsujino, H., Deushi, M., Mizuta, R., Yabu, S., Obata, A., Nakano, H., Ose T. and Kitoh, A., 2012. A new global climate model of Meteorological Research Institute: MRI-CGCM3 - Model description and basic performance. *J. Meteor. Soc. Japan, Special Issue*.

Appendix A: 90% quantiles of the CanESM2 and HadGEM2-ES models

In addition to the to the figures given in section 2.1, the results of the regridding analysis of the other two models (CanESM2 and HadGEM2-ES) are shown below.

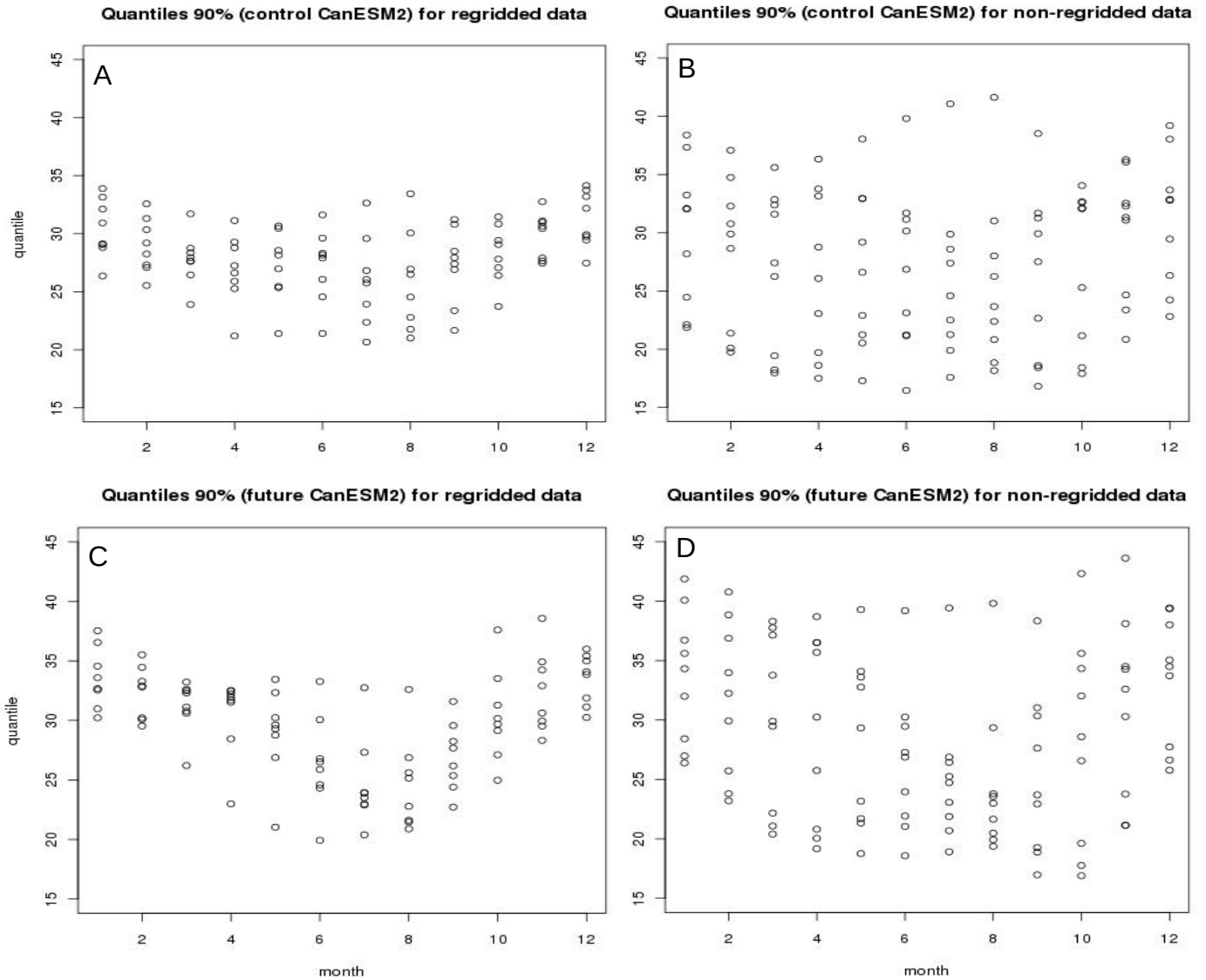


Figure 10: 90% quantile (in mm precipitation) of the CanESM2 model for the control and future period. The left panels (A and C) show the results of the regridded data (1 value per grid per month for 8 grid cells), the right panels (B and D) those for the results of the original 35 grid cells.

Probability factor 90% (control CanESM2) for regridded data **Probability factor 90% (control CanESM2) for non-regridded data**

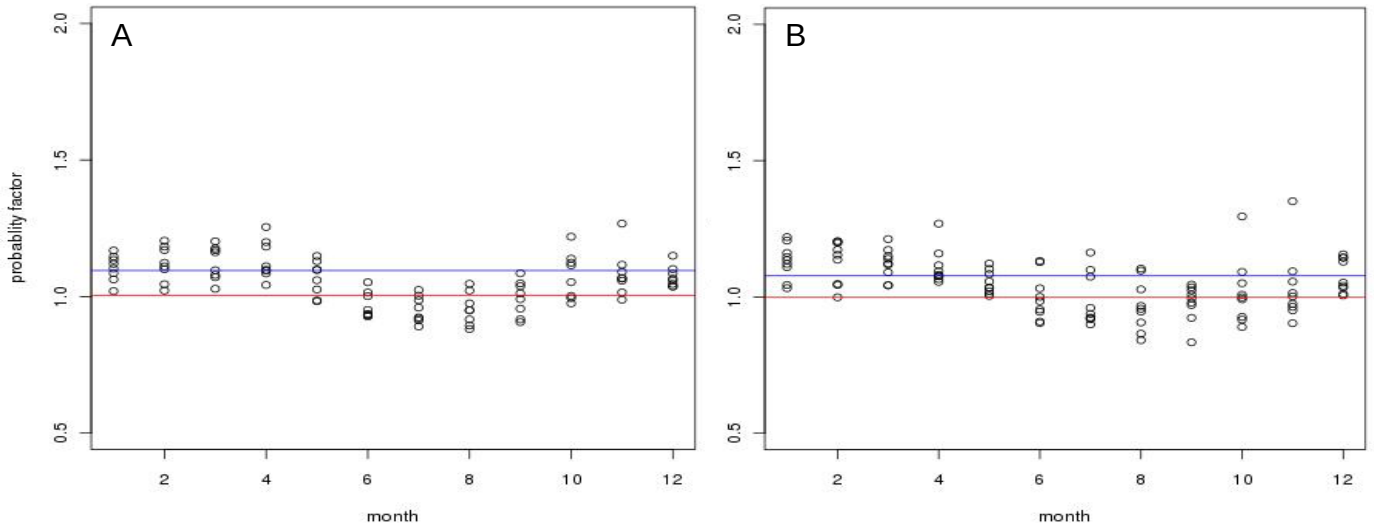


Figure 11: 90% quantile (in mm precipitation) of the CanESM2 model for the future period. The left panel (A) shows the results of the regridded data (1 value per grid per month for 8 grid cells), the right panel (B) those for the results of the original 35 grid cells.

Probability factor 90% (control HadGEM2-ES) for regridded data **Probability factor 90% (control HadGEM2-ES) for non-regridded data**

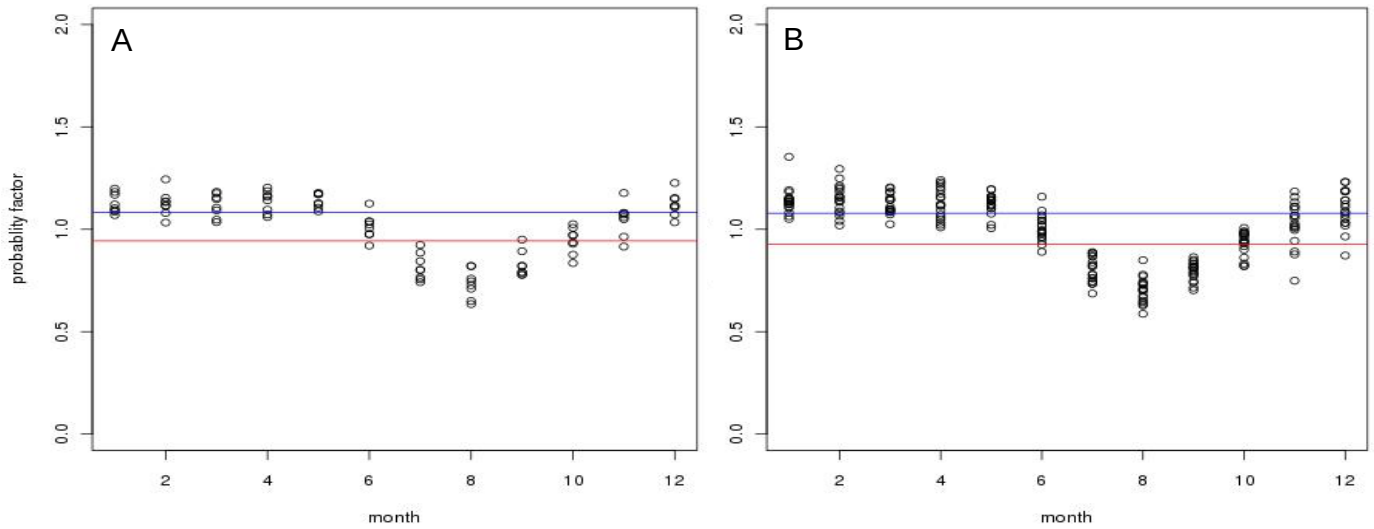


Figure 12: 90% quantile (in mm precipitation) of the HadGEM2-ES model for the future period. The left panel (A) shows the results of the regridded data (1 value per grid per month for 8 grid cells), the right panel (B) those for the results of the original 35 grid cells.

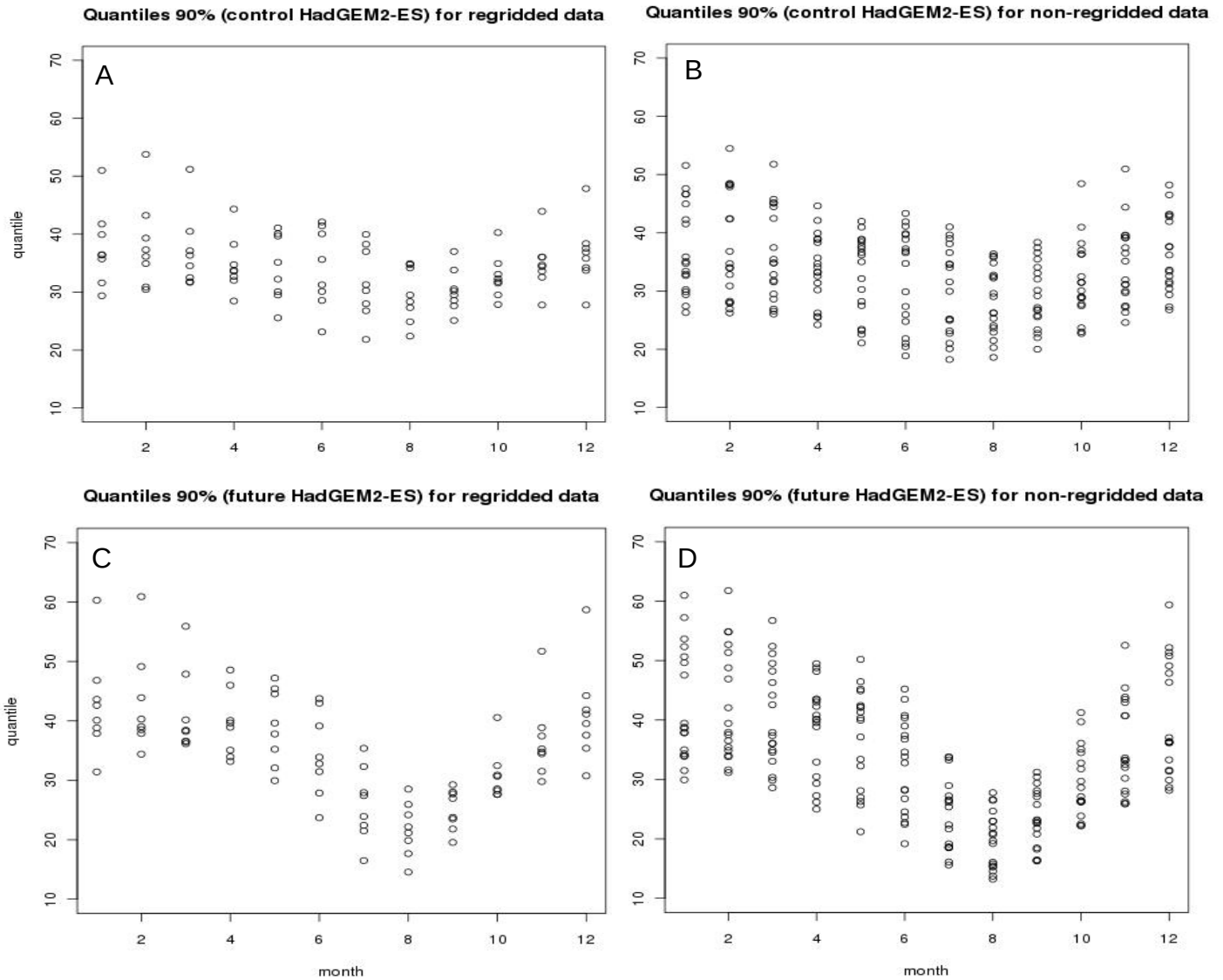


Figure 13: 90% quantile (in mm precipitation) of the HadGEM2-ES model for the control and future period. The left panels (A and C) show the results of the regridded data (1 value per grid per month for 8 grid cells), the right panels (B and D) those for the results of the original 35 grid cells.

Appendix B: Summary table for the summer period

	Summer	run	P30	P60	P90	\bar{E}	a	b
1A	bcc-csm1-1	r1i1p1	1,156	1,118	1,113	1,167	1,163	0,985
2A	CanESM2	r1i1p1	1,050	1,054	1,069	1,177	0,993	1,029
2B	CanESM2	r2i1p1	0,961	1,004	1,040	1,174	0,904	1,058
2C	CanESM2	r3i1p1	1,055	1,077	1,122	1,130	0,979	1,041
2D	CanESM2	r4i1p1	0,981	1,003	1,066	1,173	0,847	1,083
2E	CanESM2	r5i1p1	0,918	0,959	1,035	1,212	0,725	1,133
3A	CCSM4	r1i1p1	1,034	1,076	1,122	1,228	0,963	1,045
3B	CCSM4	r2i1p1	1,036	1,063	1,092	1,164	0,971	1,045
4A	CNRM-CM5	r1i1p1	1,030	1,082	1,061	1,084	1,130	0,985
5A	CSIRO-Mk3-6-0	r10i1p1	0,990	1,034	1,076	1,076	0,912	1,072
5B	CSIRO-Mk3-6-0	r1i1p1	1,013	1,058	1,091	1,077	0,952	1,043
5C	CSIRO-Mk3-6-0	r3i1p1	1,022	1,053	1,065	1,084	0,971	1,039
5D	CSIRO-Mk3-6-0	r4i1p1	0,991	1,029	1,058	1,121	0,952	1,050
5E	CSIRO-Mk3-6-0	r5i1p1	1,137	1,130	1,110	1,105	1,157	0,992
5F	CSIRO-Mk3-6-0	r6i1p1	0,988	1,021	1,071	1,171	0,901	1,056
5G	CSIRO-Mk3-6-0	r7i1p1	0,937	0,984	1,060	1,176	0,834	1,086
5H	CSIRO-Mk3-6-0	r8i1p1	1,160	1,143	1,126	1,085	1,194	0,987
5I	CSIRO-Mk3-6-0	r9i1p1	1,114	1,115	1,105	1,140	1,103	1,007
6A	FGOALS-s2	r1i1p1	1,023	1,051	1,074	1,153	0,957	1,042
6B	FGOALS-s2	r2i1p1	1,149	1,122	1,132	1,210	1,118	1,006
6C	FGOALS-s2	r3i1p1	1,035	1,067	1,092	1,169	1,008	1,026
7A	HadGEM2-ES	r1i1p1	1,000	1,035	1,078	1,130	0,931	1,074
7B	HadGEM2-ES	r2i1p1	1,246	1,162	1,133	1,030	1,261	0,970
7C	HadGEM2-ES	r3i1p1	1,137	1,136	1,125	1,118	1,119	1,009
7D	HadGEM2-ES	r4i1p1	1,052	1,104	1,117	1,146	1,027	1,037
8A	inmcm4	r1i1p1	0,954	1,032	1,054	1,128	0,992	1,028
9A	IPSL-CM5A-LR	r1i1p1	0,950	1,014	1,082	1,168	0,872	1,068
9B	IPSL-CM5A-LR	r2i1p1	0,960	1,002	1,084	1,228	0,810	1,105
9C	IPSL-CM5A-LR	r3i1p1	0,901	0,953	1,030	1,192	0,734	1,122
9D	IPSL-CM5A-LR	r4i1p1	1,044	1,073	1,123	1,175	0,949	1,057
10A	IPSL-CM5A-MR	r1i1p1	1,023	1,075	1,120	1,227	0,954	1,064
11A	MIROC-ESM	r1i1p1	1,110	1,114	1,109	1,115	1,143	0,996
12A	MIROC-ESM-CHEM	r1i1p1	1,119	1,105	1,099	1,035	1,121	0,999
13A	MPI-ESM-LR	r1i1p1	1,099	1,099	1,081	1,004	1,174	0,976
13B	MPI-ESM-LR	r2i1p1	1,086	1,106	1,107	1,083	1,093	1,012
13C	MPI-ESM-LR	r3i1p1	1,000	1,066	1,070	1,117	1,012	1,031
14A	MRI-CGCM3	r1i1p1	1,050	1,104	1,096	1,061	1,095	1,006
15A	NorESM1-M	r1i1p1	1,000	1,044	1,090	1,238	0,906	1,069
MEAN GCM's			1,040	1,065	1,089	1,139	0,998	1,038
Min GCMs			0,901	0,953	1,030	1,004	0,725	0,970
Max GCMs			1,246	1,162	1,133	1,228	1,261	1,133

Table 4: Relative changes in 30%, 60% and 90% quantiles and mean excess (resp. P30, P60, P90 and \bar{E}) for the 5-day sum summer precipitation, after transformation by delta change approach. Also the change factors a and b are included in this table and a Performance Index (Wang, 2012) is shown in the last column. The colours indicate the highest (red) and lowest (blue) 5 values of the variables.

Appendix C: Gumbel distribution for calculation of return periods

The return levels for 10-day winter maximum precipitation sums are calculated to show the influence of the transformation on extreme precipitation.

The 10-day maxima are calculated from overlapping 10-day periods (different from the 5-day sums, which are non-overlapping), starting at the 1st of October to 31st of March. This results in a total of 182 days (for the 365 day-models), so 173 10-day sums, over the winter period. From each year, the maximum 10-day sum is selected. From the total 35 year period, 34 full winter periods give 34 maximum precipitation sums. These values have been ordered and plotted in a Gumbel plot to show the return period for these precipitation amounts.

The Gumbel distribution (pers. comm. Jules Beersma and Adri Buishand) is a distribution with a location and scale parameter. A random variable (X), following the Gumbel variable can be represented as Equation (7). For the ordered values $X_1 \leq \dots \leq X_n$ and $Y_1 \leq \dots \leq Y_n$ a similar equation applies:

$$X = \mu + \sigma Y \quad (8)$$

$$X_i = \mu + \sigma Y_i \quad (9)$$

In this equation μ is the location parameter, $\sigma (>0)$ the scale parameter and Y the standard variable. For which $\mu = 0$ and $\sigma = 1$. The relation between the standard Gumbel variable Y and the standard uniform variable U_i is given by:

$$Y = -\ln(-\ln[U]) \quad (10)$$

$$Y_i = -\ln(-\ln[U_i]) \quad (11)$$

Equation (10) and (11) show the same relation between X and Y , with the exception that Equation (11) is applied for the ordered values. The standard Gumbel variable itself has a distribution function (12) which is used for a probability plot.

$$G(x) = Pr[Y < x] = \exp(-e^{-x}) \quad (12)$$

To apply this function for calculating return periods, the median of the function U_i can approximately be represented by Equation (13) which can be combined into the complete formula for a Gumbel distribution (14).

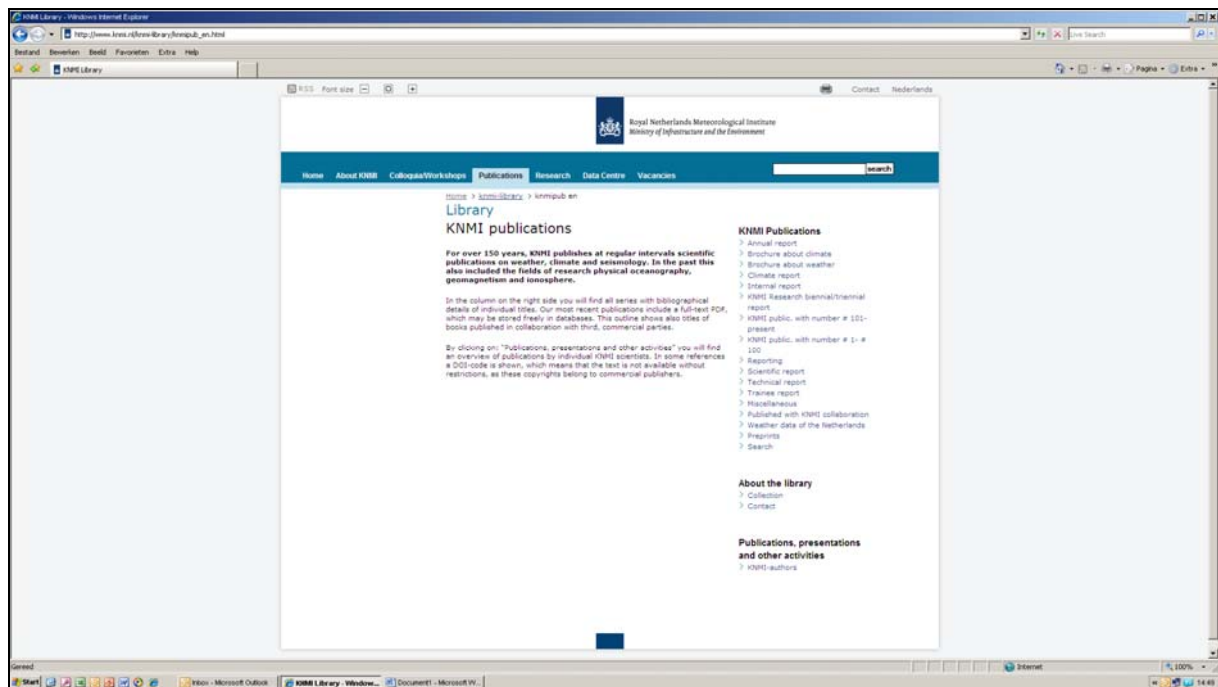
$$Med[U_i] = P_{i,n} \approx \frac{i-0.3}{n+0.4} \quad (12)$$

$$Med[Y_i] \approx -\ln\left(-\ln\left[\frac{i-0.3}{n+0.4}\right]\right) \quad (13)$$

The approximation in Equation (13) is often referred to a median plotting position. Its effect is that the return period associated to the largest value in the data corresponds to approximately 1,5 times the length of the data set (in years). For the 35-year time series of used in this study (which contain 34 complete winters) the cumulative probability for the largest winter maximum corresponds to $P = (34-0.3)/(34+0.4) = 0.97$, which in turn corresponds with a return period of $T = 1/(1-p) = 49.14$ year.

A complete list of all KNMI -publications (1854 – present) can be found on our website

www.knmi.nl/knmi-library/knmipub_en.html



The most recent reports are available as a PDF on this site.

